MATERIALS SCIENCE

Pressure-induced shear and interlayer expansion in Ti_3C_2 MXene in the presence of water

Michael Ghidiu,[1] Sankalp Kota,[1] Vadym Drozd,[2] Michel W. Barsoum[1]*

Pseudo-negative compressibility in layered materials is a phenomenon typically limited to in situ high-pressure experiments in some clay minerals and carbon-based materials. We show that the MXene $Ti_3C_2T_x$ expands along its crystallographic *c* direction when compressed in the presence of H_2O. This expansive effect occurs when a mixture of powders and excess water is quasi-hydrostatically compressed in a diamond anvil cell; it also occurs to a much larger extent when powders are pressed uniaxially into discs and, notably, persists after pressure is released. We attribute the expansion to the insertion of H_2O molecules and have identified shear-induced slipping of the nanosheets comprising multilayered MXene particles as a possible cause of this behavior in the latter case. This both has implications for the processing of MXenes and contributes to the field of materials with pseudo-negative compressibility by adding a new member for further investigation.

INTRODUCTION

The seemingly counterintuitive expansion along certain crystallographic directions of some layered materials as a result of applied compressive stress has been observed in a host of materials of varied chemistry, such as graphite oxide (GO), clay minerals, and layered titanates (*1*–*4*). The phenomenon is generally observed in situ during isostatic compression and is the result of solvent molecules (water, alcohols, or other organics) intercalating between weakly bonded layers. There are some instances where the effect is preserved, for some time, after the pressure is released (*2*). For the case of water, the entry of H_2O has been attributed to osmotic effects from ions generated by pressure-induced dissociation of surface functional groups (*2*) or, more generally, from the ability to induce a higher density of solvent inside the interlayer space than in the pressure-transmitting medium (*5*). Although the effect appears in various classes of layered materials, the exact mechanisms have not been elucidated with clarity to date.

MXenes are a recent addition to the families of hydrophilic, layered two-dimensional (2D) materials and are of the form $M_{n+1}X_nT_x$ (where M is a transition metal, X is carbon and/or nitrogen, and T is a variable surface group of -OH, -O, and -F; *n* is an integer from 1 to 3) that have been gaining momentum since their discovery in 2011 (*6*). They are promising alternatives to more well-studied materials in applications as far ranging as capacitive energy storage (*7*), electromagnetic shielding (*8*), and contaminant removal (*9*, *10*). MXenes are both hydrophilic and electrically conductive as a result of the presence of high densities of mobile electronic carriers (*11*). Their hydrophilicity renders them similar to clay minerals, as has recently been highlighted by our group (*12*, *13*) and others (*14*). For example, MXene interlayers can contain exchangeable cations that may have profound effects on various properties such as the dynamics of confined H_2O, the interlayer spacing, or conductivity (*15*–*17*). The clay-like behavior has also opened new directions for processing, such as direct production of films via rolling (*12*).

Herein, we explore cases where the MXene $Ti_3C_2T_x$ exhibits an enlarged basal spacing as a result of applied external pressure. The impetus for this work was our observation that the interlayer spacings of some $Ti_3C_2T_x$ pressed discs were significantly larger than those from the starting powders. We characterize expansion of the multilayer distances, which occurs to a large extent when compressed uniaxially and, to a small extent, when compressed quasi-hydrostatically, and attempt to elucidate the difference in behavior between these two modes of compression. We believe the addition of a new material to those that are known to exhibit this behavior to be important to the field of high-pressure studies and continuing to advance the field of MXenes.

RESULTS AND DISCUSSION

We first produced multilayered $Ti_3C_2T_x$ by etching Ti_3AlC_2 powders in 10 weight % HF. After washing and drying these powders (designated "HF10") in ambient air so that the starting hydration level of all powders was that at approximately 50% relative humidities (RHs), the resulting powders were equilibrated in various RHs via saturated salt solutions (*18*). The {00*l*} region (basal spacing, where intercalation effects are most pronounced) shows only small changes to the rather disordered structure (Fig. 1A). We note here that we have decided to break with convention and discuss structure in terms of simple basal spacing $d_{(001)}$ rather than the *c* parameter of a $P6_3/mmc$ unit cell ($2 \times d_{(002)}$) because

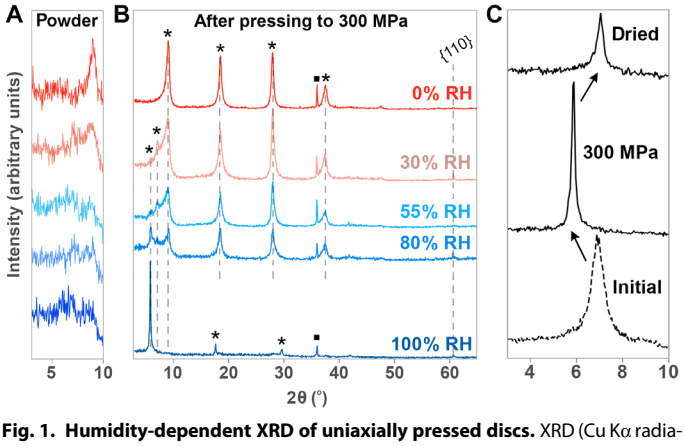

Fig. 1. Humidity-dependent XRD of uniaxially pressed discs. XRD (Cu Kα radiation) of $Ti_3C_2T_x$ equilibrated at various RHs. (**A**) Powders directly after equilibration (all reflections are {00*l*}). (**B**) Same powders, after uniaxial pressing to 300 MPa to form discs. Asterisks denote {00*l*} reflections, and squares denote (111) reflections from a small amount of TiC impurity. (**C**) Initial wet paste directly after preparation (bottom), after pressing to 300 MPa to form a disc (middle), and after drying the disc over P_2O_5 for 48 hours (top). All reflections are {00*l*}.

[1]Department of Materials Science and Engineering, Drexel University, Philadelphia, PA 19104, USA. [2]Department of Mechanical and Materials Engineering, Center for the Study of Matter at Extreme Conditions, Florida International University, Miami, FL 33174, USA. *Corresponding author. Email: barsoumw@drexel.edu

we do not know whether that symmetry is preserved in the processes described herein. In other words, equivalent values reported herein are half that of typical *c* parameters common in the MXene literature.

Upon pressing the equilibrated powders uniaxially in a 1-cm-diameter steel die to 300 MPa to form freestanding discs, intense {00*l*} peaks are observed (Fig. 1B). This increase of intensity is a normal occurrence and reflects the strong preferential alignment of multilayered, van der Waals–stacked flakes. However, it is clear that the initial equilibration humidity has a large effect on the final structure. Over the series of RH, after pressing, the basal spacing varies from ~10 to ~15 Å, with a small peak corresponding to 12.5 Å occurring in intermediate humidities. These changes correspond roughly to the size of an H_2O molecule, with 12.5 Å phases corresponding to an H_2O monolayer and 15 Å phases corresponding to a bilayer (*13*, *19*). The d_{001} of 10 Å represents a collapsed MXene structure with no H_2O (*15*).

Figure 1C gives further evidence of the involvement of H_2O. The bottom trace shows $Ti_3C_2T_x$ powders directly after preparation from etching—before any kind of drying—measured as a still-wet paste. It has been noted before that fresh $Ti_3C_2T_x$ etched with 10% HF may exhibit expanded hydrated phases that can persist until the material is allowed to dry (*9*, *20*). The fact that we observe only a 12.5 Å d_{001} in this hydrated sample, and not larger spacings, rules out the possibility that even the presence of liquid water would be enough to spontaneously swell the spacing to 15 Å. After uniaxial pressing in a steel die, the peak downshifted to 6° or a basal spacing of 15 Å (Fig. 1B). This structure was stable on a scale of at least 2 weeks in ambient atmosphere and likely longer. However, it reverted back to 12.5 Å when the disc was dried over a P_2O_5 desiccant (~0% RH) for a few days. Given the ability of MXene to intercalate water molecules (*13*), a reasonable first assumption is that the changes in basal spacing are due to the reversible insertion of H_2O as a result of applied pressure. This same conclusion can be reached by the fact that the powders equilibrated at 0% RH from Fig. 1 (A and B) start with the collapsed d_{001} of 10 Å and show no expansion after uniaxial pressing.

With these results, the multilayered $Ti_3C_2T_x$ was expected to behave like other materials that undergo pressure-induced expansion. To test this idea, multilayered $Ti_3C_2T_x$ was characterized at high pressure in a diamond anvil cell (DAC), with resulting changes in structure monitored by in situ x-ray diffraction (XRD). In the first experiment, the powders were wetted with a small amount of water to approximate conditions experienced in the pressed-disc experiments. Under these conditions, no expansion in the basal spacing was observed, only monotonic compression with applied stress. The basal spacing $d_{(001)}$ as a function of pressure is shown in Fig. 2B (black triangles). To try to observe the maximum expansion, the DAC was loaded with a large excess of water so that the multilayered MXene particles were dispersed throughout the water, which acted as a pressure-transmitting medium. The quasi-hydrostatic pressure was increased to 5 GPa and subsequently decreased while recording diffraction patterns (Fig. 2A; extracted $d_{(001)}$ values are in Fig. 2B, blue circles). A small expansion of approximately +0.3 Å from the starting point of 12.5 Å (already presumed to contain a single layer of H_2O) was observed in the low-pressure region, which is in the same pressure range experienced during the pressed-disc experiments; this was followed by normal compression, with a slope similar to that from the first DAC experiment with less H_2O. The qualitative shape of this plot is also similar to those in the aforementioned literature. Upon the removal of the stress, the basal spacing increased to ~13.2, or 0.7 Å larger than its initial value. The most likely explanation here is that there are two competing effects: pressure-induced intercalation of H_2O and compressive strain due to the applied load. After the pressure is released, the H_2O intercalated under pressure becomes apparent, leading to a higher *d* spacing than initially observed. However, despite this, the magnitude of the effect is not nearly as large as that observed in the pressed-disc results from Fig. 1 (13.2 Å versus 15 Å). Because the maximum expansion for the DAC results is smaller than the scale of an H_2O molecule, the changes in the interlayer are not simplistic in a sense of monolayer versus bilayer; given that the initial basal spacing of ~12.5 Å suggests

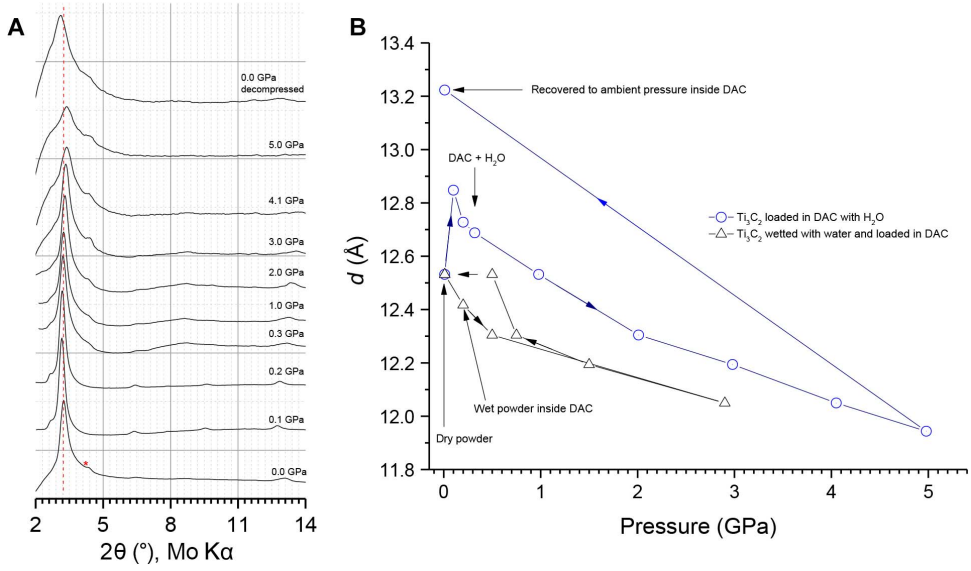

Fig. 2. Pressure-dependent in situ XRD. (**A**) XRD patterns (Mo Kα radiation) of $Ti_3C_2T_x$ collected in DAC at various pressures up to ≈5 GPa using water as pressure-transmitting medium (that is, a large excess of water). The red asterisk (*) denotes the (002) reflection of a small amount of residual Ti_3AlC_2. All other reflections are MXene {00*l*}. (**B**) Basal spacing d_{001} as a function of external pressure for $Ti_3C_2T_x$ in two experiments with different amounts of water: excess H_2O (blue circles) and a small amount of H_2O (black triangles). Note that the maximum expansion here is almost 2 Å smaller than those reported in Fig. 1.

an interlayer height of about one H_2O molecule, changes on a smaller scale could represent different orientations of the molecules or further packing of H_2O into the structure causes some expansion without supporting a bilayer. The presence of the expansive effect in the DAC results, albeit small, supports the idea that this kind of insertion can be a general phenomenon in hydrophilic layered materials (*3*). Note that the expansion of the basal spacing occurred before the solidification of the water medium—the full diffraction pattern at 2 GPa in fig. S1 shows the formation of ice VI, and that at 3 GPa in fig. S2 shows the transformation to ice VII (*21*). We note that because of the use of fine powders, the crystallization process may occur at higher pressures than the phase diagram of pure water indicates (*3*).

From a simple mechanics perspective, the main difference between the uniaxial pressing and DAC systems should be a deviatoric component of the stress. We set out to investigate the idea that this could lead to slipping of the nanosheets. Because this shear would be at a maximum at the powder/die interfaces in the uniaxial system, we attempted to characterize the internal structure of the discs as well, where these stresses are not as high. Because the x-ray penetration depth is small compared to the thickness of the discs, this was accomplished by scraping thin layers off of the discs with a razor and then running XRD on the newly exposed surfaces (the depth of material removed was determined by comparing the difference obtained from height alignments in the diffractometer). From Fig. 3A, it is clear that even in the case of 0% RH, there is high preferential orientation (along the basal direction) at the surface compared to the bulk (Fig. 3A). This alignment effect is known and discussed in the literature (*22*). However, the peak corresponding to ~10 Å persists deep within the disc, although with reduced intensity. On the other hand, the 100% RH sample's peak corresponding to a basal spacing of ~15 Å (Fig. 3B) disappears between 20 and 40 μm from the surface, with no traces of other peaks, suggesting that the ordering of the material along [001] is quite strong only at the surface (in contact with the die) and that the bulk of the pressed disc is highly variable in basal spacing. From these results, it is clear that the observed behavior is primarily a surface effect, where the multilayered particles interact with the steel die. Further evidence for this effect is in the form of material ejected through a seam and up the side of the die wall (as shown in fig. S3A). This material was carefully collected, and XRD (fig. S3B) revealed that it also had an expansion to 15 Å, despite the fact that this part of the material was oriented orthogonally to the direction of pressure and was outside of the main die body; however, because of the small size of the seam, it would certainly have experienced high shear forces.

We next turned to scanning electron microscopy (SEM) to examine the morphology of the discs, starting with the 100% RH disc, which displayed the most obvious increase in basal spacing. Figure 4A shows the microstructure of this disc's surface, whereas Fig. 4B shows the interior (after it was fractured). Not only is high alignment apparent at the surface compared to the bulk but also the particles appear to have undergone extreme slipping of the nanosheets (red arrow), leading to a surface that appears to be composed of turbostratically disordered flakes. This structure of overlapping flakes could create a stronger barrier to diffusion and may help explain why, when the disc with a basal spacing of 15 Å was dried over a desiccant, only one layer of H_2O was lost to reach 12.5 Å, rather than a fully collapsed structure at 10 Å. The particles in the bulk are disrupted as well (green arrow) but to a much lesser degree.

The surface of the 55% RH disc (Fig. 4C) shows some signs of extreme slipping in the particles (red arrow) but only in small isolated areas, whereas the surface of the 0% RH disc shows only minor effects on some particles (Fig. 4D). Combining these morphologies with the controlled-humidity XRD results, we find a strong correlation between the basal expansion in the uniaxially pressed discs and evidence of a high degree of slipping of the nanosheets. This is bolstered by SEM of the surface of the material ejected along the inside of the die (which, as XRD showed, has a d_{001} of 15 Å), also showing the same highly turbostratic morphology (fig. S3C); this part of the sample would certainly not have experienced the same kind of stress environment as the disc surface but would have experienced high shear stresses during the ejection process. No changes to the basal spacing were observed when 0% RH discs were exposed to water so the water must be present at the

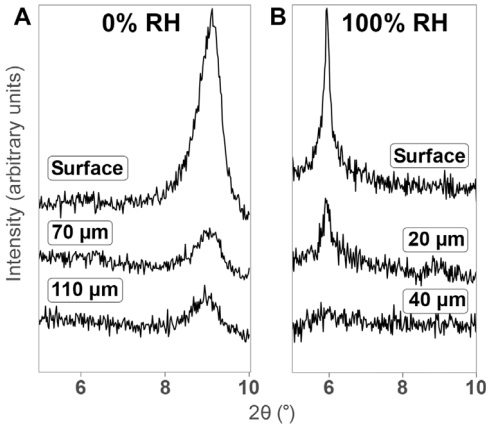

Fig. 3. Depth-profile XRD of pressed discs. XRD (Cu Kα radiation) of $Ti_3C_2T_x$ pressed into discs at 300 MPa. (**A** and **B**) Powders were equilibrated at 0% RH (A) or 100% RH (B) before pressing. In each case, further XRD was taken after indicated approximate depths of material had been removed from the surface by scraping to obtain an approximation of the depth profile. All reflections are {00*l*}.

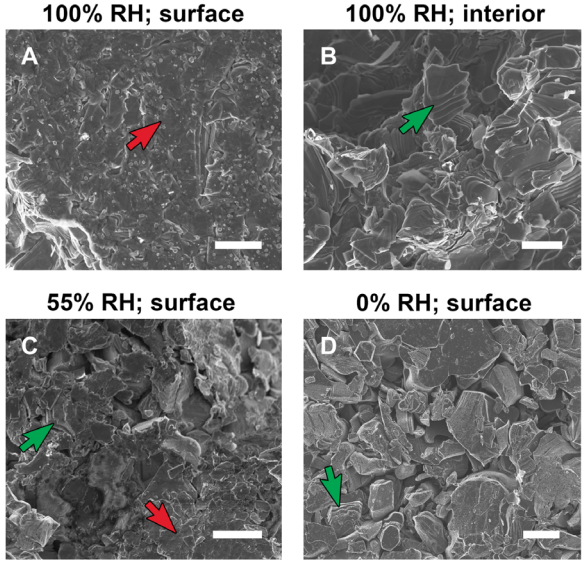

Fig. 4. SEM images of pressed-disc surfaces. SEM images of various pressed discs made with powders that had been equilibrated, before pressing, at various labeled RHs. (**A** and **B**) Images from the surface (A) and interior (B) of the same disc. Examples of multilayered particles at various states of shear are labeled with green arrows; regions of extreme shear are labeled with red arrows. Scale bars, 4 μm.

same time as pressure is applied to have an effect, possibly through increased lubricity of the sheets, facilitating movement. Clay minerals that exhibit expansion under pressure have been observed to also have sheet-to-sheet slip effects (*3*), but the authors in that study did not comment on a possible causal relationship to expansion.

The presence of ions in the MXene interlayer, specifically K^+, reduce H_2O mobility and "glue" the MXene sheets together (*15*). To test this, we prepared $Ti_3C_2T_x$ intercalated with K^+ (*13*). When the powders were equilibrated at various humidities and pressed into the discs at 300 MPa as before, the final basal spacing was no longer a function of RH and, instead, remained at a constant ~12.5 Å (Fig. 5A). Further, even the sample equilibrated at 100% RH did not show evidence of sheet slippage in SEM after pressing into a disc (Fig. 5B). Therefore, we conclude that the presence of K^+ ions inhibits the behavior observed in Fig. 4, and any expansive behavior that may persist after pressure is released.

In GO, one explanation for the phenomenon of expansion under pressure is pressure-induced proton transfer (*23*, *24*) leading to the dissociation of surface groups according to Talyzin *et al.* (*2*)

$$\text{R-OH} + H_2O = \text{R-O}^- + H_3O^+$$

followed by intercalation of H_2O due to osmotic pressure. Further, reports have suggested that pressure-induced insertion may be a general phenomenon for layered hydrophilic materials (*3*). MXenes are both hydrophilic and have OH surface groups, so the fact that some expansion was observed in situ in the presence of excess water may be attributed to a similar phenomenon. However, it seems evident that nanosheet slippage in multilayered $Ti_3C_2T_x$ in the presence of H_2O is the only way to achieve full long-lasting expansion to 15 Å. It may be that the separation of multilayered $Ti_3C_2T_x$ particles into disordered sheets breaks the sheet-to-sheet bonding that allows for each face of the sheet to become hydrated. This is a significant result because this phenomenon may represent a way to circumvent the irreversibility of dehydration under ambient conditions for $Ti_3C_2T_x$ lacking intercalated cations (*20*).

Table 1 compares the basal spacings of a number of $Ti_3C_2T_x$ films/discs produced by various methods. Production of multilayered $Ti_3C_2T_x$ using 10% HF alone yields a basal spacing of 13.5 Å (before drying) and ~10 Å (after drying). However, when the multilayered stacks are delaminated into flakes and restacked, they restack with H_2O to yield nearly the same *d* spacing observed in the pressed discs from this work (that is, 15.1 Å). Previous work from our groups with a different etching system, HCl + LiF (in situ HF generation rather than using HF directly), yields the same spacing when pressed into discs (using the same conditions as this work) (*12*). Other techniques, such as spray coating, also showed similar basal spacings at 14.75 Å (*25*). Further, reports of thick films produced by filtering $Ti_3C_2T_x$ flake suspensions display the same *c* lattice parameter before drying (*26*). Finally, work on single flakes measured by atomic force microscopy, with a layer of H_2O between MXene and substrate, shows a height of 15 ± 2 Å per flake (*27*).

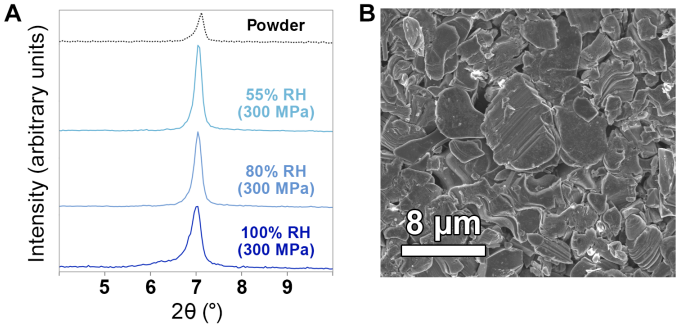

Fig. 5. Humidity-dependent ex situ XRD after K^+ intercalation. Effect of K^+ ions intercalated into $Ti_3C_2T_x$. (**A**) XRD of $Ti_3C_2T_x$ discs pressed at 300 MPa from powders that were equilibrated at various relative humidities. All reflections are MXene {00*l*}. (**B**) SEM micrograph of the top surface of the 100% RH disc, showing no evidence of major nanosheet slipping.

In general, the basal spacings of multilayered $Ti_3C_2T_x$ reported in the literature are quite variable and depend on processing conditions. Nevertheless, and with the exception of the first two rows, the systems in Table 1 display nearly identical values. The commonality between all of these systems is a separation of flakes in the presence of H_2O, leading to the hydration of the flake surfaces. This has precedent in other 2D literature, for example, MoS_2 that, when delaminated in the presence of H_2O, has its basal planes hydrated by a layer of H_2O, which remains when the material is restacked (*28*).

Table 2 compares the lattice expansion of other layered solids that display in situ pressure-induced expansion. Note that Δd is not trivial to define because the expansion may be defined from the baseline of a prehydrated phase or from that of the fully collapsed structure. For clarity, we have included both in Table 2. For $Ti_3C_2T_x$, after pressure was applied, the change in *d* spacing measured from the fully collapsed structure (that is, with no intercalated water) is +5 Å, corresponding to a bilayer of H_2O. The change from the initially hydrated phase (that is, from Fig. 1B) is +2.5 Å, or insertion of an additional monolayer. Thus, with the exception of kaolinite (which started as a partially expanded hydrated phase), the expansion in other cases is due to the pressure-induced insertion of an additional monolayer of H_2O, and the values are similar to those reported in this work. As far as we are aware, this large, shear-induced, long-lasting expansion of hydrophilic van der Waals–layered materials reported herein has not been reported to date. On a final note to this discussion, there has been work on pressure-induced hydration of zeolites, where structural changes caused by high pressure can cause changes to pore shape, leading to increased accessibility of H_2O in the high-pressure state (*29*). We leave this as a possible alternative mechanism and suggest exploration into it in further study for MXenes; the relatively weak interlayer bonding in MXene may allow for changes in the structure of the interlayer space under pressure that increases accessibility to H_2O. In the case that these changes are caused by sheet slippage, the increased lubricity from intercalated H_2O could be a cooperative effect.

One practical concern for these results is in the area of electrical conductivity. A common way to report the conductivity of MXenes in powder form [especially samples that cannot be delaminated to form films, or at least not without surfactants which may be difficult to later remove (*30*)] has been to press them into freestanding discs for measurement (*17*, *22*, *31*). Given, from this work, that the humidity of the environment may play a large role in affecting conductivity through basal spacing modulation, interparticle contact, and degree of turbostratic disorder (as well as the depth to which this disorder occurs), more care will need to be taken in the future when reporting conductivity results. Last, given the interest in processing of MXenes by rolling/shearing (*12*), this work can hopefully provide some insight and help guide future studies on processes that might

Table 1. Comparison of basal spacings of $Ti_3C_2T_x$ made by different methods.

Etching system	Processing	Basal spacing (Å)	Δd_{001} (Å)*	Reference
10% HF	Undisturbed multilayered stacks, dry	~10†	0	(*6*, *22*)
10% HF	Undisturbed multilayered stacks, still wet	13.5†	3.5	(*9*)
10% HF	Delaminated and restacked	15.1†	5.1	(*9*)
HCl + LiF	Disc (pressed at 300 MPa)	15.0‡	5	(*12*)
HCl + LiF	Spray-coated film (from delaminated suspension)	14.75†	4.75	(*25*)
HCl + LiF	Thick film via filtration of delaminated suspension	15.2†	5.2	(*26*)
HCl + LiF	Spincoating (single- to few-layer flakes)	15 ± 2§	5	(*27*)
10% HF	Disc (pressed at 300 MPa)	15	5	This work

*Measured as the expansion from fully collapsed dry structure with d_{001} = 10 Å. †Pressed-disc data not included in published report. ‡From reported $d_{(002)}/2$. §Monolayer with H_2O via atomic force microscopy.

Table 2. Compilation of basal spacings of pressure-induced expansion in materials in the literature.

Material	Δd_{001} (Å)	Pressure (GPa)	Reference
$Ti_3C_2T_x$	2.5*/5†	0.3 (uniaxial, ex situ)‡	This work
	0.16*/2.66†	0.32 (quasi-hydrostatic)§	
	0.69*/3.19†	After unloading from 4.98 (quasi-hydrostatic)	
Na-fluorohectorite (a clay mineral)	2*	2.5 (hydostatic)§	(*34*)
Kaolinite	1.5*/2.4†	0.1 (hydrostatic, over 65 hours)§	(*35*)
GO	2.5*/6.9†	1.25 (hydrostatic)§	(*1*)

*Δd defined as difference between the phase after pressure is applied and highest d spacing observed from ambient-pressure hydration. †Δd defined as difference between pressure-hydrated phase and dried, fully collapsed structure. ‡Maximum pressure applied (ex situ experiments). §Pressure at which the expansion was observed to occur.

increase lubricity to ease the shearing of MXene multilayered particles into rolled films.

CONCLUSIONS

The basal spacings of $Ti_3C_2T_x$ multilayered MXene expanded significantly when sheared in the presence of water. The shearing appears to facilitate the insertion of a bilayer of water between the sheets, which may be due to overcoming an energy barrier required to break sheet-to-sheet bonds and allow access of H_2O to the basal surfaces. Intercalated K^+ ions appear to inhibit this effect. When compressed hydrostatically in a large excess of water, the MXene does show expansion, in line with other hydrophilic layered materials; however, the effect, although potentially involving the insertion of H_2O molecules, is smaller than that observed from uniaxially pressed discs. Thus, there may be two phenomena at play: expansion caused by increased accessibility of H_2O due to nanosheet slippage and expansion under hydrostatic conditions caused by as-yet unconfirmed phenomena. Further study is needed for clarification.

MATERIALS AND METHODS

$Ti_3C_2T_x$ synthesis

The MAX phase Ti_3AlC_2, precursor to $Ti_3C_2T_x$, was pressureless-sintered from powders of Ti_2AlC and TiC at 1350°C for 2 hours, following methods reported previously (*13*). Multilayered $Ti_3C_2T_x$ was produced by etching the Al layers from Ti_3AlC_2 by one of two methods, both established in the literature: either (i) by immersing Ti_3AlC_2 powders (<38 μm particle size) in 10% HF for 22 hours, followed by washing, referred to as HF10; or (ii) "HF + LiCl," the same as (i), except with the addition of LiCl to the etchant in a Ti_3AlC_2/LiCl ratio of 1:5 mol, which was then ion-exchanged with KCl to yield K^+-intercalated MXene (*13*, *20*).

Pressed discs

The $Ti_3C_2T_x$ powders were equilibrated in sealed plastic bags containing a desiccant (P_2O_5, ~ 0% RH), distilled water (100% RH), or saturated salt solutions at 25°C for humidity control according to well-established protocols (*18*). The powders were allowed to equilibrate for 7 days, after which they were quickly removed, placed in a stainless steel cylindrical

die with a diameter of 1 cm, and compressed to a load corresponding to a stress of 300 MPa. The loading and unloading rates were approximately 300 MPa/min, with no additional hold time at the maximum pressure.

XRD of pressed discs

XRD was performed on a powder diffractometer (Rigaku SmartLab) using Cu Kα radiation in the Bragg-Brentano configuration. Samples were scanned at a step size of 0.02° to 0.04° and dwell time of 1 s per step.

High-pressure XRD

DAC experiments were performed using a symmetrical cell and diamond anvils of 900-μm culet size. A 350-μm-thick beryllium bronze gasket was pre-indented to a thickness of 150 μm. The pressure chamber was a 300-μm hole drilled in the gasket. The pressure was determined from the fluorescence shift of small ruby crystals within the pressure chamber (*32*). XRD patterns at high pressure were collected using a General Area Detector Diffraction System (GADDS)/D8 diffractometer (Bruker) equipped with a SMART APEX charge-coupled device detector and a direct-drive molybdenum rotating anode (MAC Science Co.) with λ = 0.71073 Å. 2D diffraction images were integrated using FIT2D (*33*). Two high-pressure experiments, using different amounts of water, were carried out. The first was performed by wetting dry $Ti_3C_2T_x$ powder with enough water to make a paste before loading into the DAC. The second was carried out by using water as a pressure-transmitting medium, that is, a large excess of water (approximately equal volumes of MXene and water).

Scanning electron microscopy

The top and facture surfaces of pressed discs were imaged using a Zeiss SUPRA 50 VP field emission scanning electron microscope.

SUPPLEMENTARY MATERIALS

Supplementary material for this article is available at http://advances.sciencemag.org/cgi/content/full/4/1/eaao6850/DC1

fig. S1. Full diffraction pattern of $Ti_3C_2T_x$ compressed in excess H_2O at a pressure of 2 GPa.
fig. S2. Full diffraction pattern of $Ti_3C_2T_x$ compressed in excess H_2O at a pressure of 3 GPa.
fig. S3. Analysis of material ejected from the side of the die.

REFERENCES AND NOTES

1. A. V. Talyzin, V. L. Solozhenko, O. O. Kurakevych, T. Szabó, I. Dékány, A. Kurnosov, V. Dmitriev, Colossal pressure-induced lattice expansion of graphite oxide in the presence of water. *Angew. Chem. Int. Ed.* **47**, 8268–8271 (2008).
2. A. V. Talyzin, B. Sundqvist, T. Szabó, I. Dékány, V. Dmitriev, Pressure-induced insertion of liquid alcohols into graphite oxide structure. *J. Am. Chem. Soc.* **131**, 18445–18449 (2009).
3. S. You, D. Kunz, M. Stöter, H. Kalo, B. Putz, J. Breu, A. V. Talyzin, Pressure-induced water insertion in synthetic clays. *Angew. Chem.* **125**, 3983–3987 (2013).
4. S. Nakano, T. Sasaki, K. Takemura, M. Watanabe, Pressure-induced intercalation of alcohol molecules into a layered titanate. *Chem. Mater.* **10**, 2044–2046 (1998).
5. E. V. Vakarin, A. V. Talyzin, On the mechanism of negative compressibility in layered compounds. *Chem. Phys.* **369**, 19–21 (2010).
6. M. Naguib, M. Kurtoglu, V. Presser, J. Lu, J. Niu, M. Heon, L. Hultman, Y. Gogotsi, M. W. Barsoum, Two-dimensional nanocrystals produced by exfoliation of Ti_3AlC_2. *Adv. Mater.* **23**, 4248–4253 (2011).
7. V. M. Hong Ng, H. Huang, K. Zhou, P. S. Lee, W. Que, J. Z. Xua, L. B. Kong, Recent progress in layered transition metal carbides and/or nitrides (MXenes) and their composites: Synthesis and applications. *J. Mater. Chem. A* **5**, 3039–3068 (2017).
8. M. Han, X. Yin, H. Wu, Z. Hou, C. Song, X. Li, L. Zhang, L. Cheng, Ti_3C_2 MXenes with modified surface for high-performance electromagnetic absorption and shielding in the X-band. *ACS Appl. Mater. Interfaces* **8**, 21011–21019 (2016).
9. Y. Ying, Y. Liu, X. Wang, Y. Mao, W. Cao, P. Hu, X. Peng, Two-dimensional titanium carbide for efficiently reductive removal of highly toxic chromium(VI) from water. *ACS Appl. Mater. Interfaces* **7**, 1795–1803 (2015).
10. Q. Peng, J. Guo, Q. Zhang, J. Xiang, B. Liu, A. Zhou, R. Liu, Y. Tian, Unique lead adsorption behavior of activated hydroxyl group in two-dimensional titanium carbide. *J. Am. Chem. Soc.* **136**, 4113–4116 (2014).
11. T. Ouisse, M. W. Barsoum, Magnetotransport in the MAX phases and their 2D derivatives: MXenes. *Mater. Res. Lett.* **5**, 365–378 (2017).
12. M. Ghidiu, M. R. Lukatskaya, M.-Q. Zhao, Y. Gogotsi, M. W. Barsoum, Conductive two-dimensional titanium carbide "clay" with high volumetric capacitance. *Nature* **516**, 78–81 (2014).
13. M. Ghidiu, J. Halim, S. Kota, D. Bish, Y. Gogotsi, M. W. Barsoum, Ion-exchange and cation solvation reactions in Ti_3C_2 MXene. *Chem. Mater.* **28**, 3507–3514 (2016).
14. J. Luo, W. Zhang, H. Yuan, C. Jin, L. Zhang, H. Huang, C. Liang, Y. Xia, J. Zhang, Y. Gan, X. Tao, Pillared structure design of MXene with ultralarge interlayer spacing for high-performance lithium-ion capacitors. *ACS Nano* **11**, 2459–2469 (2017).
15. N. C. Osti, M. Naguib, A. Ostadhossein, Y. Xie, P. R. C. Kent, B. Dyatkin, G. Rother, W. T. Heller, A. C. T. van Duin, Y. Gogotsi, E. Mamontov, Effect of metal ion intercalation on the structure of MXene and water dynamics on its internal surfaces. *ACS Appl. Mater. Interfaces* **8**, 8859–8863 (2016).
16. G. R. Berdiyorov, K. A. Mahmoud, Effect of surface termination on ion intercalation selectivity of bilayer $Ti_3C_2T_2$ (T = F, O and OH) MXene. *Appl. Surf. Sci.* **416**, 725–730 (2017).
17. M. Ghidiu, S. Kota, J. Halim, A. W. Sherwood, N. Nedfors, J. Rosen, V. N. Mochalin, M. W. Barsoum, Alkylammonium cation intercalation into Ti_3C_2 (MXene): Effects on properties and ion-exchange capacity estimation. *Chem. Mater.* **29**, 1099–1106 (2017).
18. L. B. Rockland, Saturated salt solutions for static control of relative humidity between 5° and 40° C. *Anal. Chem.* **32**, 1375–1376 (1960).
19. A. Lerf, R. Schoellhorn, Solvation reactions of layered ternary sulfides A_xTiS_2, A_xNbS_2, and A_xTaS_2. *Inorg. Chem.* **16**, 2950–2956 (1977).
20. H.-W. Wang, M. Naguib, K. Page, D. J. Wesolowski, Y. Gogotsi, Resolving the structure of $Ti_3C_2T_x$ MXenes through multilevel structural modeling of the atomic pair distribution function. *Chem. Mater.* **28**, 349–359 (2016).
21. A. V. Talyzin, B. Sundqvist, T. Szabó, V. Dmitriev, Structural breathing of graphite oxide pressurized in basic and acidic solutions. *J. Phys. Chem. Lett.* **2**, 309–313 (2011).
22. M. Naguib, O. Mashtalir, J. Carle, V. Presser, J. Lu, L. Hultman, Y. Gogotsi, M. W. Barsoum, Two-dimensional transition metal carbides. *ACS Nano* **6**, 1322–1331 (2012).
23. N. Koifman, B. Cohen, D. Huppert, Effect of pressure on proton-transfer rate from a photoacid to ethanol solution. *J. Phys. Chem. A* **106**, 4336–4344 (2002).
24. A. U. Ortiz, A. Boutin, K. J. Gagnon, A. Clearfield, F.-X. Coudert, Remarkable pressure responses of metal–organic frameworks: Proton transfer and linker coiling in zinc alkyl gates. *J. Am. Chem. Soc.* **136**, 11540–11545 (2014).
25. K. Hantanasirisakul, M.-Q. Zhao, P. Urbankowski, J. Halim, B. Anasori, S. Kota, C. E. Ren, M. W. Barsoum, Y. Gogotsi, Fabrication of $Ti_3C_2T_x$ MXene transparent thin films with tunable optoelectronic properties. *Adv. Electron. Mater.* **2**, 1600050 (2016).
26. C. E. Ren, K. B. Hatzell, M. Alhabeb, Z. Ling, K. A. Mahmoud, Y. Gogotsi, Charge- and size-selective ion sieving through $Ti_3C_2T_x$ MXene membranes. *J. Phys. Chem. Lett.* **6**, 4026–4031 (2015).
27. M. Mariano, O. Mashtalir, F. Q. Antonio, W.-H. Ryu, B. Deng, F. Xia, Y. Gogotsi, A. D. Taylor, Solution-processed titanium carbide MXene films examined as highly transparent conductors. *Nanoscale* **8**, 16371–16378 (2016).
28. P. Joensen, E. D. Crozier, N. Alberding, R. F. Frindt, A study of single-layer and restacked MoS_2 by X-ray diffraction and X-ray absorption spectroscopy. *J. Phys. C Solid State Phys.* **20**, 4043 (1987).
29. Y. Lee, J. A. Hriljac, T. Vogt, J. B. Parise, G. Artioli, First structural investigation of a super-hydrated zeolite. *J. Am. Chem. Soc.* **123**, 12732–12733 (2001).
30. M. Naguib, R. R. Unocic, B. L. Armstrong, J. Nanda, Large-scale delamination of multi-layers transition metal carbides and carbonitrides "MXenes." *Dalton Trans.* **44**, 9353–9358 (2015).
31. J. Yang, M. Naguib, M. Ghidiu, L.-M. Pan, J. Gu, J. Nanda, J. Halim, Y. Gogotsi, M. W. Barsoum, Two-dimensional Nb-based M_4C_3 solid solutions (MXenes). *J. Am. Ceram. Soc.* **99**, 660–666 (2016).
32. H. K. Mao, P. M. Bell, J. W. Shaner, D. J. Steinberg, Specific volume measurements of Cu, Mo, Pd, and Ag and calibration of the ruby R_1 fluorescence pressure gauge from 0.06 to 1 Mbar. *J. Appl. Phys.* **49**, 3276–3283 (1978).
33. A. P. Hammersley, S. O. Svensson, M. Hanfland, A. N. Fitch, D. Hausermann, Two-dimensional detector software: From real detector to idealised image or two-theta scan. *High Press. Res.* **14**, 235–248 (1996).
34. S. You, D. Kunz, M. Stöter, H. Kalo, B. Putz, J. Breu, A. V. Talyzin, Pressure-induced water insertion in synthetic clays. *Angew. Chem. Int. Ed.* **52**, 3891–3895 (2013).

35. N. Wada, R. Raythatha, S. Minomura, Pressure effects on water-intercalated kaolinite. *Solid State Commun.* **63**, 783–786 (1987).

Acknowledgments: We thank the Drexel Centralized Research Facilities for the help in materials characterization. We thank S. Saxena (Florida International University) for the contributions to the manuscript and experimental analysis. **Funding:** This material is based on work supported by the NSF Graduate Research Fellowship Program under grant no. 283036-3304 (to M.G.). Any opinions, findings, and conclusions or recommendations expressed in this material are those of the authors and do not necessarily reflect the views of the NSF. M.W.B. was supported by the Swedish Research Council (621-2014-4890).
Author contributions: M.G., S.K., and M.W.B. were responsible for the ex situ experiments and analysis. V.D. was responsible for the in situ experiments and analysis. **Competing interests:** The authors declare that they have no competing interests. **Data and materials availability:** All data needed to evaluate the conclusions in the paper are present in the paper and/or the Supplementary Materials. Additional data related to this paper may be requested from the authors.

Submitted 15 August 2017
Accepted 8 December 2017
Published 12 January 2018
10.1126/sciadv.aao6850

Citation: M. Ghidiu, S. Kota, V. Drozd, M. W. Barsoum, Pressure-induced shear and interlayer expansion in Ti_3C_2 MXene in the presence of water. *Sci. Adv.* **4**, eaao6850 (2018).

ScienceAdvances

Pressure-induced shear and interlayer expansion in Ti_3C_2 MXene in the presence of water

Michael Ghidiu, Sankalp Kota, Vadym Drozd and Michel W. Barsoum

Sci Adv **4** (1), eaao6850.
DOI: 10.1126/sciadv.aao6850

Science Advances

AAAS

advances.sciencemag.org/cgi/content/full/4/1/eaao6850/DC1

Supplementary Materials for

Pressure-induced shear and interlayer expansion in Ti_3C_2 MXene in the presence of water

Michael Ghidiu, Sankalp Kota, Vadym Drozd, Michel W. Barsoum

Published 12 January 2018, *Sci. Adv.* **4**, eaao6850 (2018)
DOI: 10.1126/sciadv.aao6850

This PDF file includes:

- fig. S1. Full diffraction pattern of $Ti_3C_2T_x$ compressed in excess H_2O at a pressure of 2 GPa.
- fig. S2. Full diffraction pattern of $Ti_3C_2T_x$ compressed in excess H_2O at a pressure of 3 GPa.
- fig. S3. Analysis of material ejected from the side of the die.

Supplementary Materials

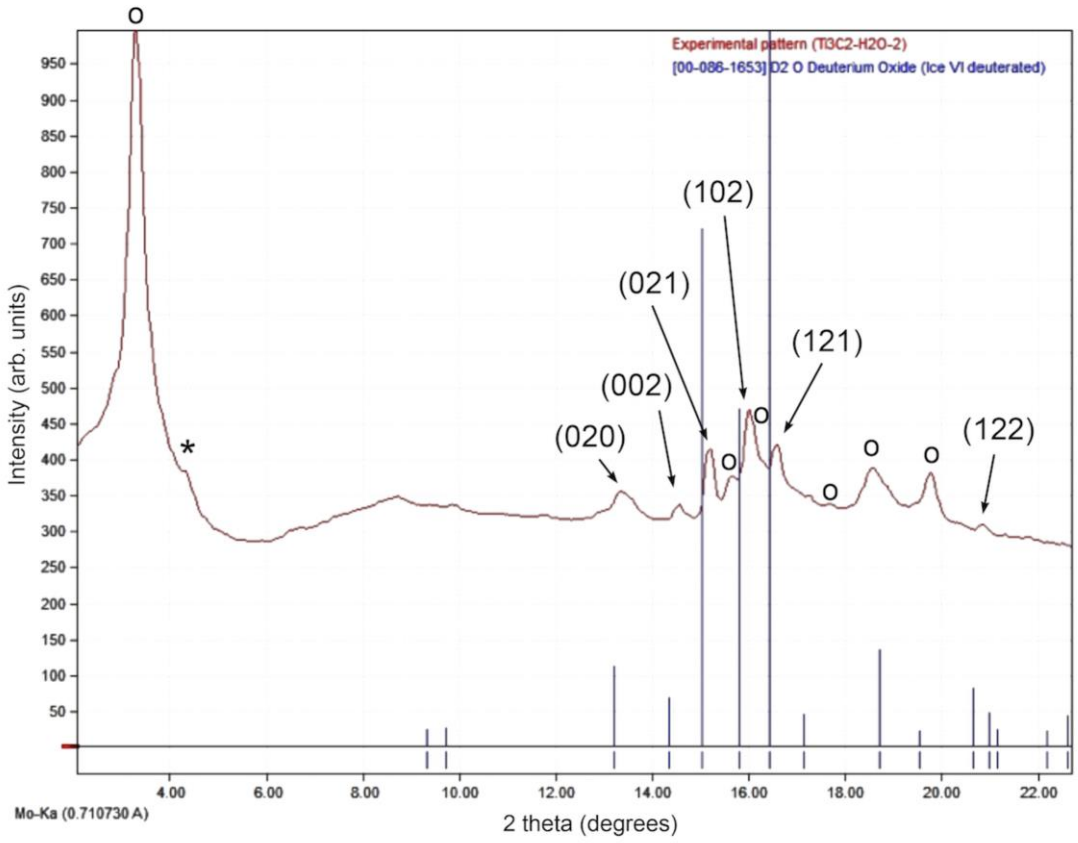

fig S1. Full diffraction pattern of $Ti_3C_2T_x$ compressed in excess H_2O at a pressure of 2 GPa. The asterisk denotes the (002) peak of a small amount of Ti_3AlC_2 impurity. Open circles denote reflections from the MXene $Ti_3C_2T_x$, in order from left to right: {00*l*}, (011), (013), (015), (016), (017). Lines represent the standard of D_2O Ice VI; the experimental peaks are shifted to higher angle because the standard is at 1.1 GPa and the experimental pattern is at 2 GPa. JCPDS standard for Ice-VI (#086-16531; 225K, 1.1GPa). Ice-VI reflections are indexed.

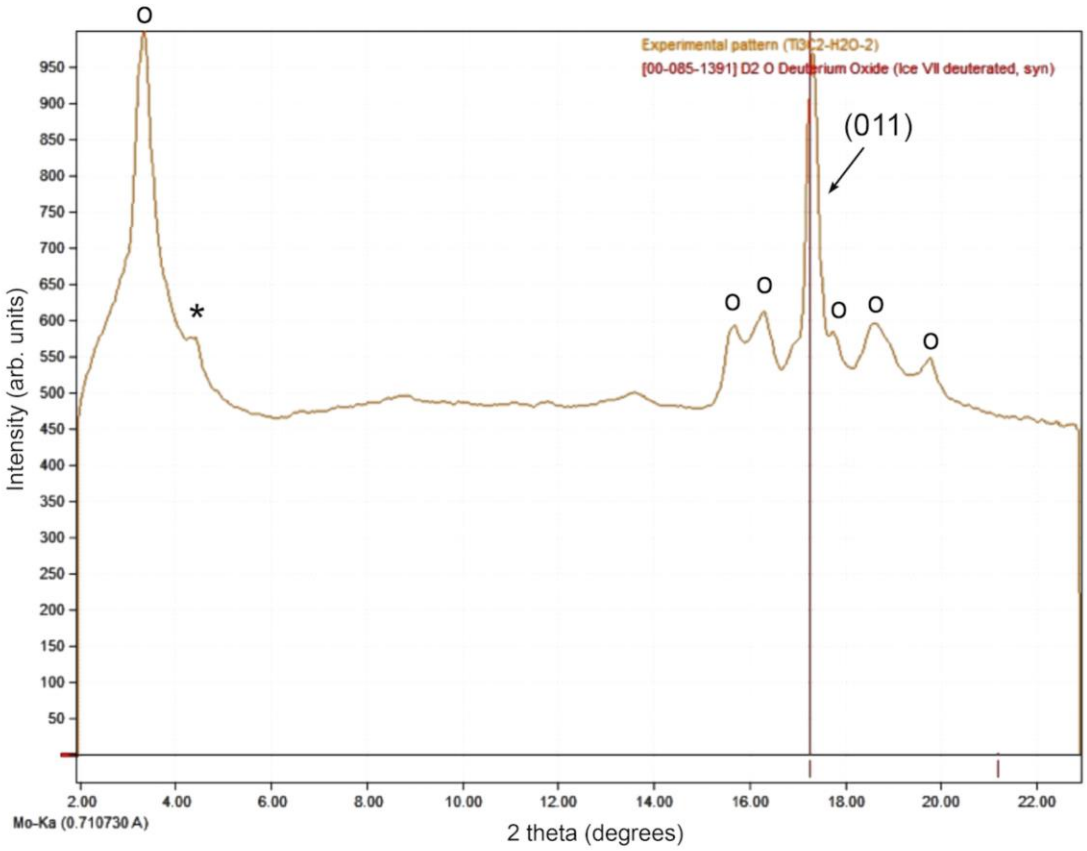

fig S2. Full diffraction pattern of $Ti_3C_2T_x$ compressed in excess H_2O at a pressure of 3 GPa. The asterisk denotes the (002) peak of a small amount of Ti_3AlC_2 impurity. Open circles denote reflections from the MXene $Ti_3C_2T_x$, in order from left to right: {00*l*}, (011), (013), (015), (016), (017). Lines represent the standard of D_2O Ice VII; the experimental peaks are shifted to higher angle because the standard is at 2.6 GPa and the experimental pattern is at 3 GPa. JCPDS standard for Ice-VII (#085-1391; 296K, 2.6GPa). Ice-VII reflections are indexed.

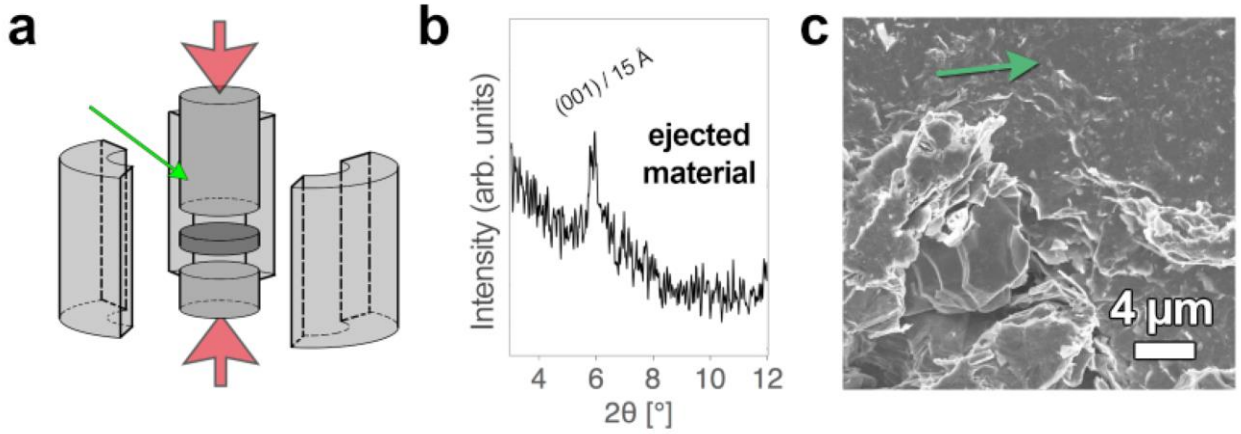

fig S3. Analysis of material ejected from the side of the die. (**A**) Schematic showing the setup of disc pressing in a steel die with 3-part walls. The large arrows indicate the direction of the uniaxial pressure, and the small arrow shows the location of MXene collected that was ejected from the main pressing area and up along the inside of the die walls. The MXene disc is shown in dark grey at the center. (**B**) XRD of the same material, showing the same expansion as observed on the surface of the disc. (**C**) SEM image of the collected material, showing large areas with nanosheets that have slipped relative to each other into a turbostratically-disordered surface.